ELSEVIER

Polymer Degradation and Stability 77 (2002) 465–475

Polymer Degradation and Stability

www.elsevier.com/locate/polydegstab

Photo-oxidation effects on mechanical properties of epoxy matrixes: Young's modulus and hardness analyses by nano-indentation

P. Delobelle[a], L. Guillot[b], C. Dubois[b,*], L. Monney[b]

[a]*LMARC UMR 6604 CNRS, UFR ST, 24 rue de l'Epitaphe, 25030 Besançon Cedex, France*
[b]*LMN/EA 473/LRC-CEA M07, UFR ST, 16 route de Gray, 25030 Besançon Cedex, France*

Received 2 February 2002; accepted 2 March 2002

Abstract

The influence of photo-oxidation on Young's modulus (E) and hardness (H) variations of two epoxy matrixes (DGEBA-MTHPA and DGEBA-IPDA) has been investigated using a Nano-Indentation test. The results show that these mechanical properties increase with irradiation time for both systems and continuously decrease with the indentation depth. These decreases are characteristic of the presence of a hard film on a softer substrate [Int. J. Solids Struct. 24 (1988) 1287]. Indeed, it was shown that the photo-degradation of these polymers leads to the formation of a thin photo-oxidation layer at the matrix's surface.

1. Introduction

In order to best optimize the use of epoxy matrixes in composite materials or in other forms, it is necessary to understand their behaviour when they are exposed to photo-oxidative conditions. In the literature, it was shown that the chemical degradation of these matrixes occurrs through their progressive removal by loss of volatile photo-oxidation products [2]. After a few hundred hours, the removal showed a linear evolution versus the light energy of irradiation [3,4]. This phenomenon revealed the progressive formation of a thin photo-oxidation layer near the irradiated surface, which then spatially advances into the organic matrix at the same speed as the ablation.

In this work, we attempted using Nano-Indentation experiments, to highlight the photo-oxidation effects on the evolution of the two main mechanical properties of the materials, i.e. Young's modulus E and the hardness H. The tests were performed on two epoxy systems (DGEBA-MTHPA and DGEBA-IPDA) that were artificially photo-aged.

2. Experimental

2.1. Materials

The epoxy matrixes were obtained from a Bisphenol A diglycidyl ether resin epoxy (DGEBA) (Scheme 1).

The first matrix was cured using methyltetrahydrophthalic anhydride as hardener (MTHPA, system I), and the second with a cycloaliphatic diamine hardener, 3-aminomethyl-3,5,5-trimethylcyclohexylamine or Isophorone diamine (IPDA, system II). The cross-linking of system I was initiated by an imidazole accelerator.

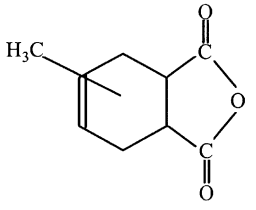

MTHPA

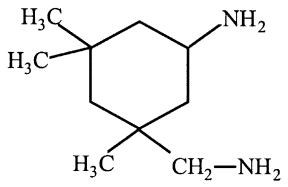

IPDA

Table 1 shows the ratio by weight (%) for both epoxy systems [5,6].

2.2. Artificial photo-ageing

Systems I and II were artificially photo-aged in a Suntest© CPS Heraeus cell [7]. They were irradiated

* Corresponding author. Tel.: +33-381-666-503; fax: +33-381-666-522.
E-mail address: claude.dubois@univ-fcomte.fr (C. Dubois).

0141-3910/02/$ - see front matter
PII: S0141-3910(02)00104-0

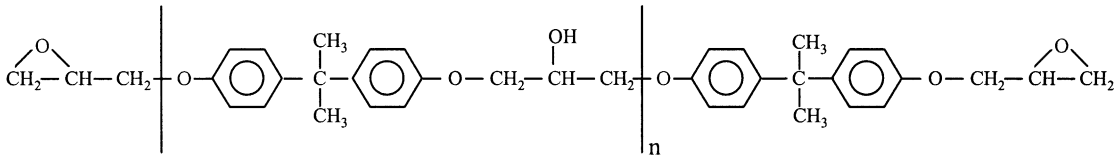

Scheme 1. Bisphenol A diglycidyl ether resin epoxy (DGEBA)

Table 1
Compounds that make up the epoxy systems

Epoxy system	Compounds	Ratio by weight (%)
I	Resin: DGEBA (CIBA Araldite LY 556)Diglicyl ether of Bisphenol A	52.4
DGEBA-MTHPA	Hardener: MTHPA (CIBA HY 917)Methyltetrahydrophthalic anhydride	47.1
	Accelerator: imidazole (CIBA DY 070)	0.5
II	Resin: DGEBA (CIBA Araldite LY 556)Diglicyl ether of Bisphenol A	81.3
DGEBA-IPDA	Hardener: IPDA (CIBA HY 2962)Isophorone diamine or 3-aminomethyl-3, 5, 5-trimethylcyclohexylamine	18.7

between 300 and 800 nm using a Xenon arc lamp, since solar radiation outside these limits does not reach the earth's surface. Samples were irradiated under an average light energy E_L of 85 ± 5 W m^{-2}. Irradiation times for both epoxy systems were:

System I (DGEBA-MTHPA):
$t=0$, 25, 48, 72, 96, 213, 246, 309, 412 and 530 h.

System II (DGEBA-IPDA):
$t=0$, 100, 200, 300, 506, 994, 1993 and 2500 h.

3. Nano-indentation

3.1. Mechanical properties

The mechanical properties measured most frequently using the load and depth sensing indentation techniques are the elastic modulus E and the hardness H. In a commonly used method, data are obtained from one complete cycle of loading and unloading (Fig. 1) [8].

The parameters noted in Fig. 1 are: P_{max} the peak indentation load, h_{max} the indenter displacement at the peak load, h_f the final depth of the contact impression after unloading and S the initial unloading stiffness.

The unloading data are then analyzed using a model for the deformation of an elastic half space by an elastic punch, which links the contact area at the peak load to the elastic modulus. Methods for independently estimating the contact area from the indenter shape function are then used to provide separate measurements of E and H [8].

For a Berkovich-type indenter, the hardness H was calculated from the relation:

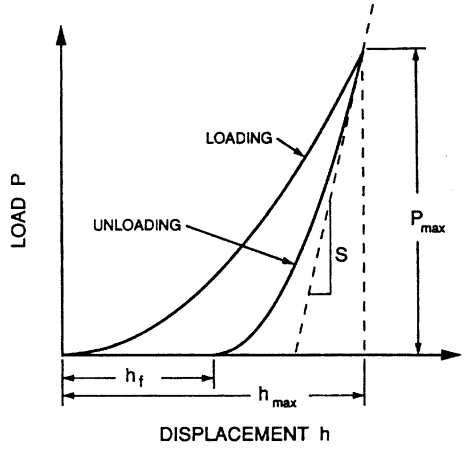

Fig. 1. Schematic representation of a loading–unloading cycle versus the indenter displacement data for an indentation experiment [8].

$$H=\frac{P}{A}\text{with } A=f(h)=24.5h^2+\sum_{n=1/2,1,2\ldots}^{6}a_n h^{1/2n} \quad (1)$$

P: applied load,
A: projected contact area,
h: indentation depth.
$\sum_{n=1/2,1,2\ldots}^{6}a_n h^{1/2n}$: geometric correction of the indenter shape, performed for the very weak displacements.

Note that an elastic correction linked to the elastic displacement recovered during the unloading is made for each hardness measurement [8].

Young's modulus E is determined from the initial unloading stiffness $S=\frac{dP}{dh}$ (Fig. 1) through the equation:

$$E_r=\frac{\sqrt{\pi}}{2\beta\sqrt{A}}\frac{dP}{dh}\text{ with }\frac{1}{E_r}=\frac{(1-\nu^2)}{E}+\frac{(1-\nu_i^2)}{E_i} \quad (2)$$

E_r: composite modulus including the indenter E_i and the matrix being studied E, ν_i, ν: Poisson coefficients for the indenter and the matrix under test, respectively.

The standard Poisson coefficient $\nu = 0.3$ was chosen, because it is a standard value for organic polymers. $\beta = 1.034$ for a triangular tip shape.

3.2. Indentation procedure

The tests were performed on a Nano-Indenter II^s. In this experiment, a diamond Berkovich-type indenter tip was forced into the matrix being studied under continuous conditions [9]. The indentation depth was linked to the contact area between the indenter and the material under test. This procedure allows the mechanical properties of the sample to be investigated and can provide data to calculate the hardness H and Young's modulus E [1,8,10,11]. The calculation is made by making an indentation with a well-controlled force P while continuously monitoring and measuring the displacement, h, of the indenter.

During the entire indentation procedure, the continuous measurement of the contact stiffness S was accomplished by applying a small oscillation to the displacement signal at relatively high frequency (45 Hz). The amplitude of the displacement oscillation was kept sufficiently small, in our case 1.5 nm, so that the deformation process was not affected by its addition. The corresponding force oscillation was monitored at the excitation frequency using a two-channel phase-sensitive detector [8]. It is thus possible to continuously measure the contact stiffness S between the sample and the indenter and to deduce the hardness H and the Young's modulus E of the studied matrix.

In our experiment, the maximum indentation depth was fixed at 1800 nm, except for some tests that were performed at up to 3000 nm. Fifteen indentation tests were performed for each sample on a $300 \times 300\ \mu m^2$ area.

4. Results and discussion

4.1. System I: DGEBA-MTHPA

The artificial photo-ageing of system I was conducted over 530 h of irradiation. Fig. 2 shows an example of the load–displacement curve versus the indentation depth h (after the irradiation time $t = 246$ h). The non-linearity is mainly due to the change of the contact area during the indenter penetration and to the viscoelastic properties of the sample.

Figs. 3 and 4 show the evolution of E and H versus the indentation depth of system I (after irradiation time $t = 246$ h). The small points represent the E or H data, which corresponds to one indentation experiment. The black points are the means with their standard deviation calculated from all the indentation tests after 246 h of irradiation for h = 100, 250, 500, 1000, 1500 and 1800 nm.

Two hundred and fifty-three indentations were made for the DGEBA-MTHPA matrix according to the procedure described above. Young's modulus E and hardness

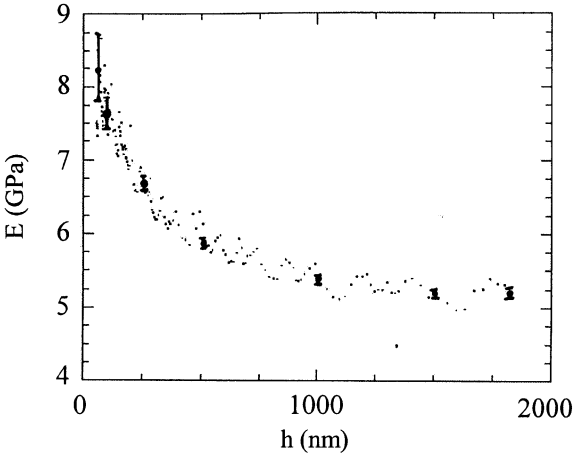

Fig. 3. E versus h ($t = 246$ h).

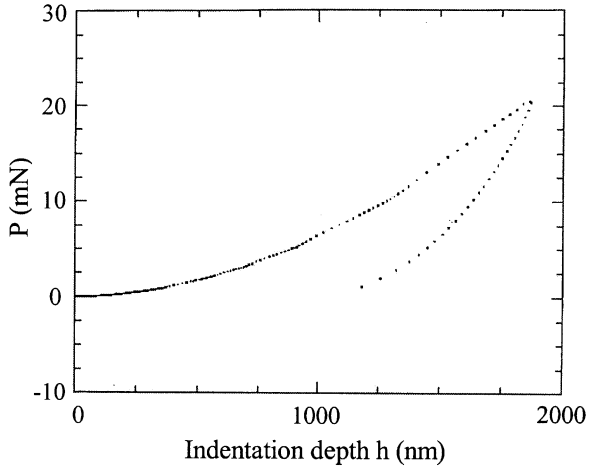

Fig. 2. Example of load–displacement curve ($t = 246$ h).

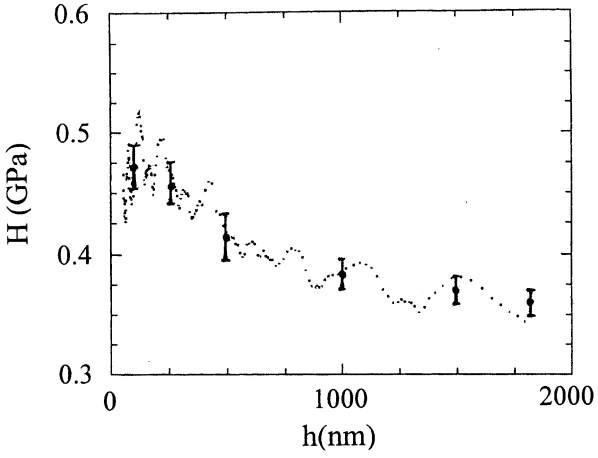

Fig. 4. H versus h ($t = 246$ h).

H versus the indentation depth h after different irradiation times t are presented in Figs. 5 and 6.

For a better legibility, these figs. do not represent all the measured points, in contrast to Figs. 9 and 10. Moreover, Fig. 5, the curve noted "plateau" corresponds to a mean obtained from the data measured at $t = 213$, 246, 309, 412 and 530 h. Indeed, after about 200–250 h of irradiation, no change appears, which confirms previous physico-chemical analyses [3,4,12–14].

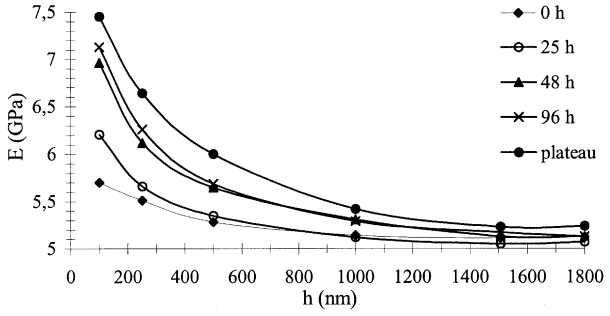

Fig. 5. E versus h (after different irradiation times)—System I.

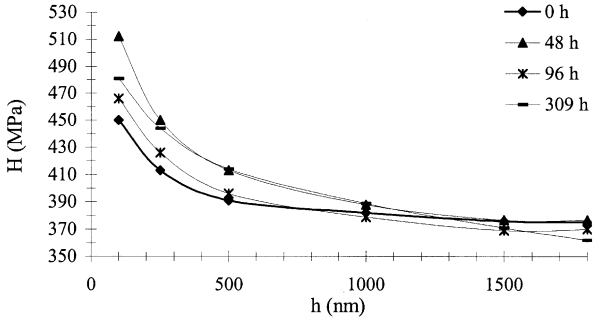

Fig. 6. H versus h (after different irradiation times)—System I.

The standard deviation for Young's modulus continuously decreased from 0.45 GPa ($h = 100$ nm) to 0.05 GPa ($h = 3000$ nm). Concerning the hardness, the standard deviation decreased from 49 MPa ($h = 100$ nm) to 3 MPa ($h = 3000$ nm). These decreases in the standard deviations probably express the weak part of the surface roughness in the measurements for the strong indentation depth. But, the previous surface roughnesses were not quantified.

In Figs. 5 and 6, Young's modulus and hardness evolution for $t = 0$ h and $h > 200$ nm (to avoid roughness effects on the measurements) are representative of the bulk mechanical properties of system I. Thus, the non-irradiated matrix presents the following characteristics:

Young's modulus: $E_{0\,I} = 5.1 \pm 0.05$ GPa
Hardness: $H_{0\,I} = 370 \pm 3$ MPa

According to Figs. 5 and 6, Young's modulus and hardness continuously decrease with the indentation depth h and increase with the irradiation time. Thus, the photo-oxidation of the DGEBA-MTHPA matrix increases the elastic and inelastic (decreases of E and H with h, respectively) properties of the matrix's surface. These decreases are characteristic of a material including two phases: a hard film on a softer substrate [1,15], i.e., in our case, a photo-oxidation layer on the non-oxidised matrix, respectively. Indeed, it was shown that the photo-ageing of the DGEBA-MTHPA matrix induced the formation of a thin photo-oxidation layer in which the degradation occurred [3,4,12–14].

Moreover, for the large indentation depth ($h \geqslant 2000$ nm), the E and H values converge, whatever the irradiation time, to be about equal to the $E_{0\,I}$ and $H_{0\,I}$ values of the non-oxidised matrix corresponding to the

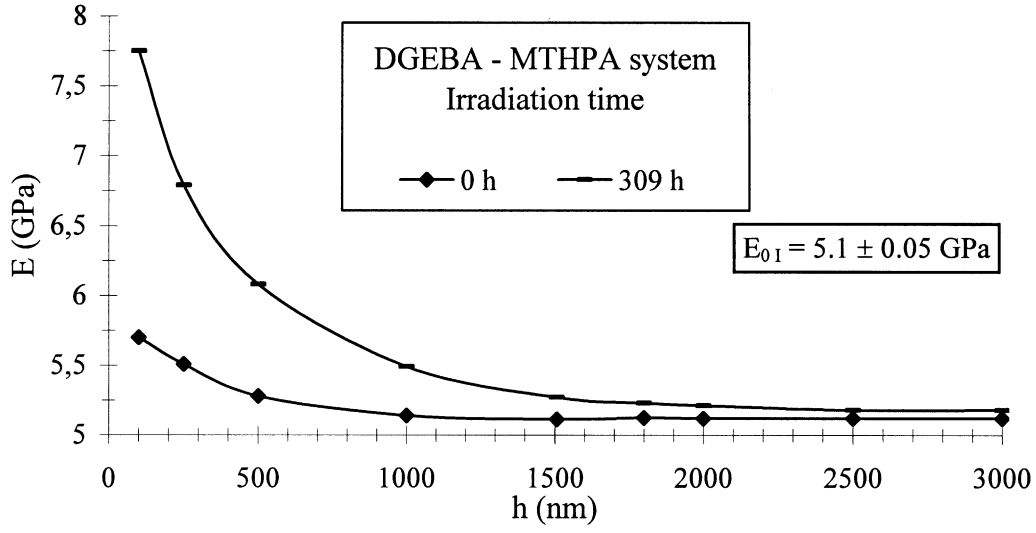

Fig. 7. Example of Young's modulus evolution up to a high indentation depth (3000 nm).

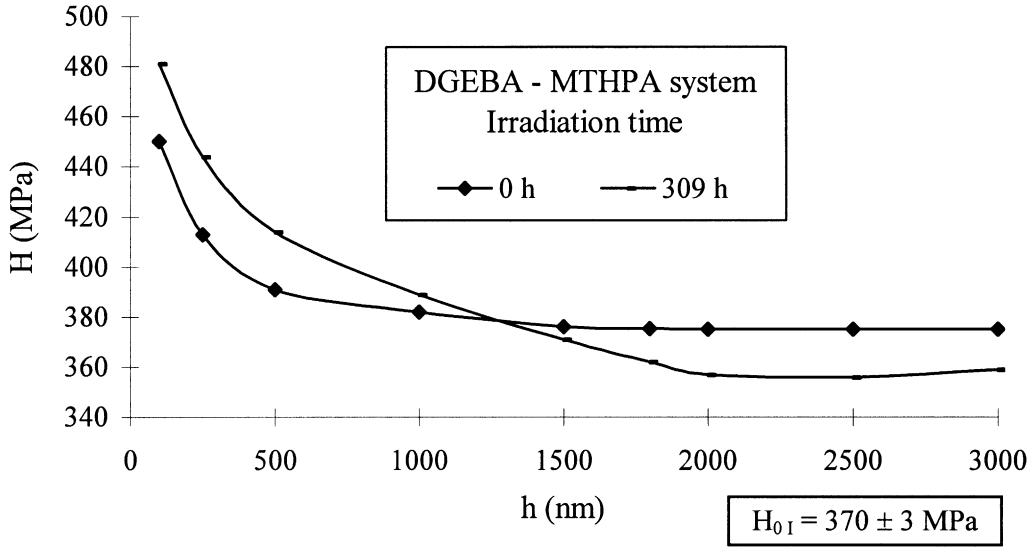

Fig. 8. Example of the hardness evolution up to a high indentation depth (3000 nm).

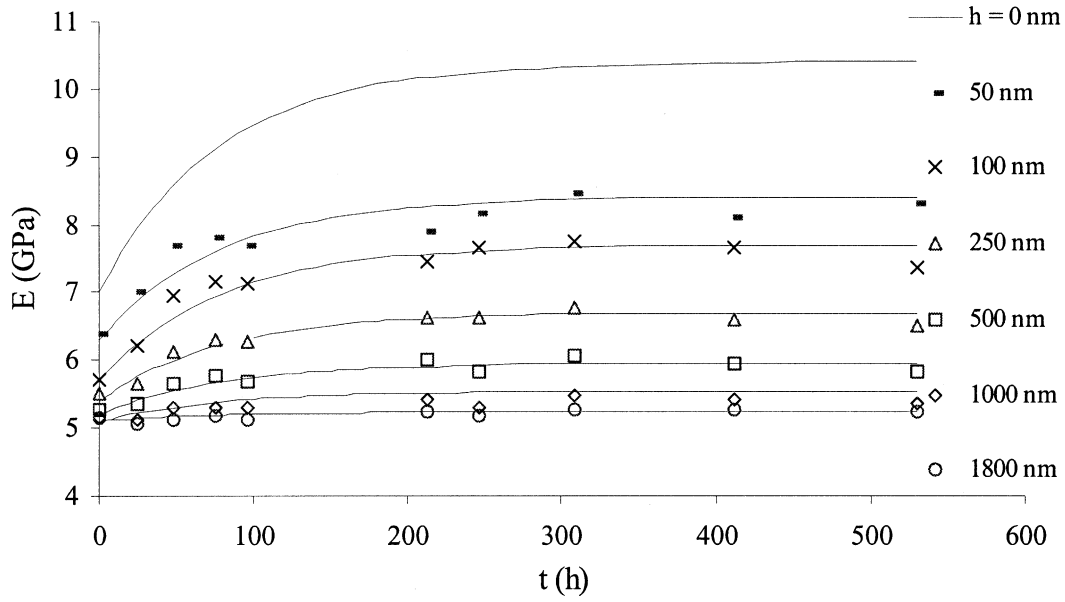

Fig. 9. E versus the irradiation time (different indentation depths)—System I (-, x, Δ, □, ◇, ○: experimental points; curves: model).

bulk properties (Figs. 7 and 8). These indentations were carried out at up to 3000 nm for $t = 0$, 309 and 530 h of irradiation.

These results show that the effects of photo-ageing on the mechanical properties of the analyzed system are mainly located in a thin photo-oxidation layer. Indeed, according to the evolution of the mechanical properties, the convergence of the curves (Figs. 5–8) with that of the bulk made it possible to estimate this thickness at about 1.8 μm. This is in good accordance with the photo-oxidation layer's thickness of the DGEBA-MTHPA system previously estimated at about 1.8–2 μm by IR-ATR spectroscopy [12].

As for the evolution of the mechanical properties with the irradiation time, Figs. 9 and 10 represent the evolutions of E and H versus t for different indentation depths h, respectively. The results show a very fast increase in the studied parameters during the first 100 h, and a saturation phenomenon clearly appears at about 250 hours of photo-ageing in regard to the standard deviation. That means that the photo-degradation of this system takes place in two successive steps: the establishment of the photo-oxidation layer, which then spatially advances at the same speed as the ablation [3,4]. Thus, the evolution of the surface's layer resulting from the removal of the organic matrix during the artificial photo-ageing process is well described from a mechanical point of view.

Note that, in Fig. 9, the calculated evolution for $h = 0$ nm has been presented as a rough guide. Moreover, for both figures, the calculated evolution has been reported

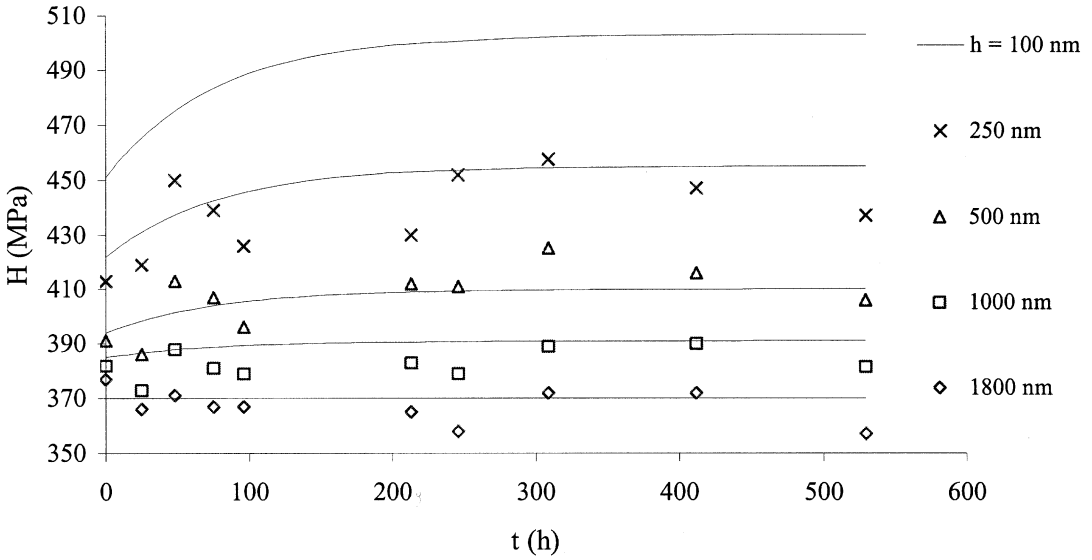

Fig. 10. H versus the irradiation time (different indentation depths)—System I (x, Δ, □, ◇: experimental points; curves: model).

for each indentation depth. These evolutions were calculated from a model described in Section 5 and correspond to Eqs. (8), (9) for E, and (13), (14) for H.

4.2. System II: DGEBA-IPDA

The study of system II was carried out following the same protocol applied to system I. The photo-ageing was conducted over 2500 h and 142 indents were made.

Figs. 11 and 12 represent the evolution of Young's modulus and hardness, respectively, versus the indentation depth h after different irradiation times. The standard deviation for Young's modulus continuously decreased from 1.13 GPa ($h=100$ nm) to 0.1 GPa ($h=3000$ nm). Concerning the hardness, the standard deviation decreased from 123 MPa ($h=100$ nm) to 10 MPa ($h=3000$ nm). These standard deviations are higher than they were for system I, probably due to a difference of previous surface roughnesses (not characterized).

As previously observed for the first system, E and H decreased with the indentation depth h and increased with the irradiation time. Thus, the DGEBA-IPDA matrix behaves similarly to system I under photo-oxidative conditions, i.e. the formation of a hard film (photo-oxidation layer) on a softer substrate (matrix).

Like the first system, it is possible to estimate in Figs. 11 and 12, the mechanical properties of the bulk matrix. The characteristics of the non-aged DGEBA-IPDA system were found to be (rough values):

Young's elasticity modulus: $E_{0\ II}=4.6\pm0.1$ GPa
Hardness: $H_{0\ II}=370\pm10$ MPa

The evolution for both mechanical parameters to a high indentation depth (3000 nm) are presented in Figs. 13 and 14.

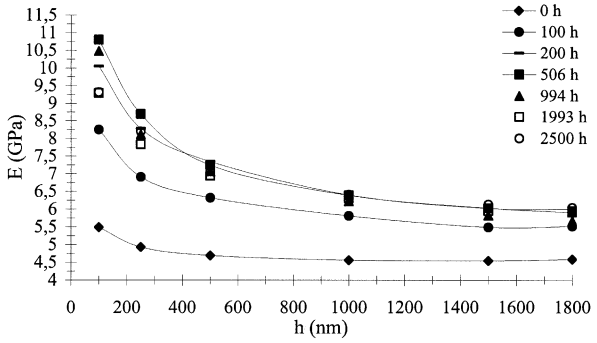

Fig 11. E versus h (after different irradiation times)—System II.

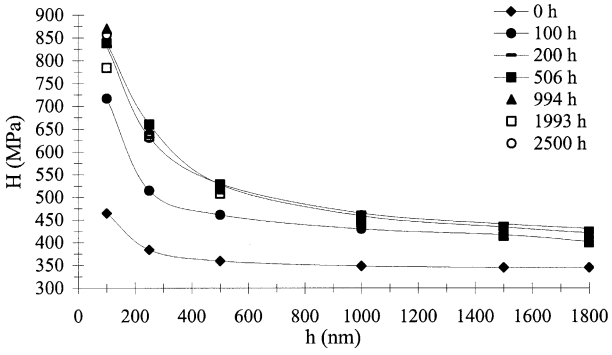

Fig 12. H versus h (after different irradiation times)—System II.

These results show that the thickness of the established photo-oxidation layer can be estimated at about 2.5–3 μm, according to the standard deviation.

Figs. 15 and 16 present the evolution of E and H versus the irradiation time for several indentation depths. Like system I, the increase in E and H is very fast for the first 100 hours of irradiation and then saturates after 250–300 h.

Note that Figs. 15 and 16 represent the calculated evolution of the studied parameters from the model described in Section 5. Previous experiments performed on these two epoxy systems showed the linear behaviour of their ablation under photo-oxidative conditions [3,4]. Moreover, the IR-ATR analyses carried out on the DGEBA-MTHPA matrix [12] prove that the photo-degradation process mainly occurred in a thin and quickly established photo-oxidation layer at the matrix's surface.

In this paper, the Nano-Indentation experiments show, for both analysed systems, the formation and the presence of this layer through the characterization of a hard film on a softer substrate. Moreover, the evolution of Young's modulus with the irradiation time highlights the chemical modifications at the matrix's surface. This study, based on the evolution of two mechanical properties, is thus in strong agreement with the previous physico-chemical analyses.

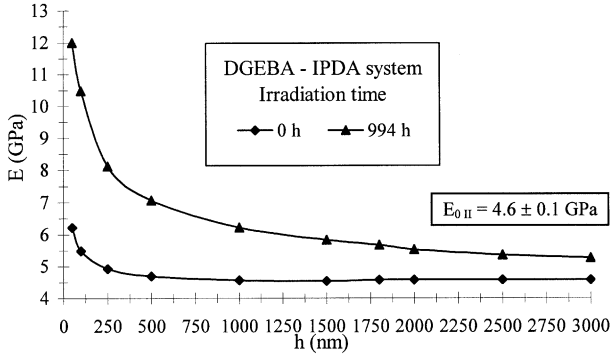

Fig. 13. Example of Young's modulus evolution up to a high indentation depth (3000 nm).

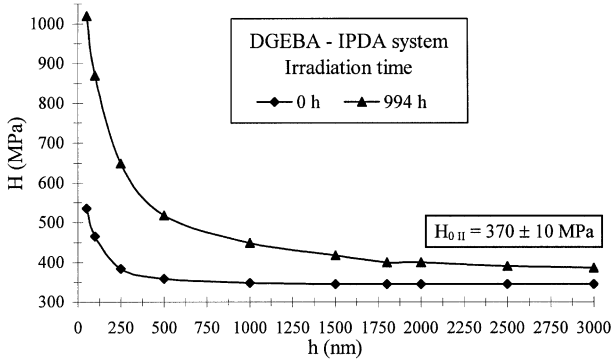

Fig. 14. Example of hardness evolution up to a high indentation depth (3000 nm).

5. Quantitative analysis of Young's modulus and hardness evolution

5.1. *Young's modulus* E

The curves in Figs. 5 and 9 (system I) and in Figs. 11 and 15 (system II) show a gradient of evolution of E versus the indentation depth and the irradiation time. In regard to these results, we have searched to establish a "law of evolution" for Young's modulus versus the irradiation time t and the indentation depth h: $E(t, h)$.

Figs. 5, 6, 11 and 12 show the decreases in E and H with h. These gradients are characteristic of a thin hard film on a softer substrate [1,15]. Thus, the intrinsic values of the film are obtained when $h \to 0$, and those of the substrate when $h >> f_t$ (f_t = film thickness).

In that case, the equivalent measured modulus can be approximated by the following equation [1,15]:

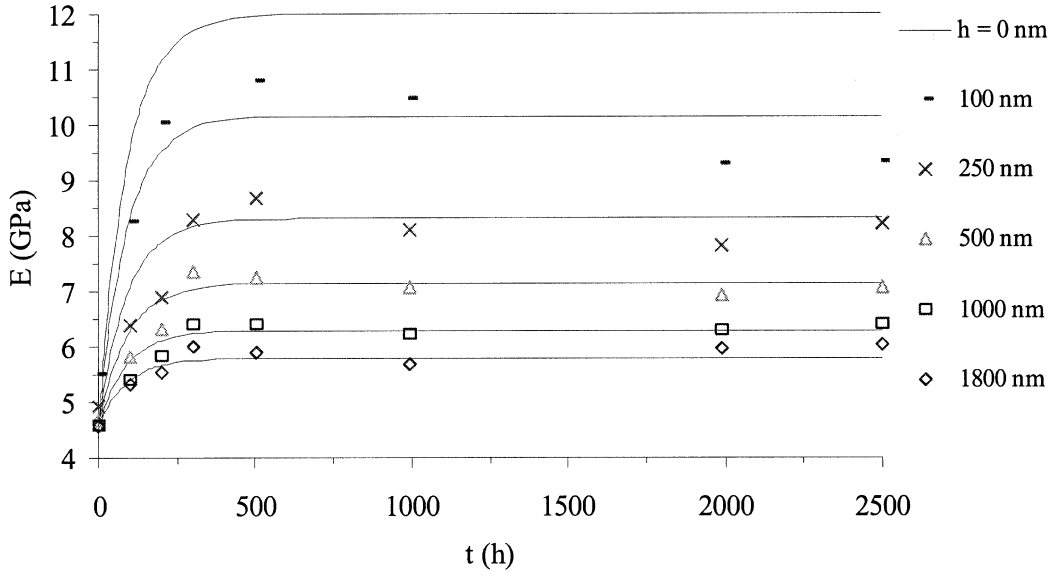

Fig. 15. E versus the irradiation time (different indentation depths)—System II. (-, x, Δ, □, ◇: experimental points; curves: model).

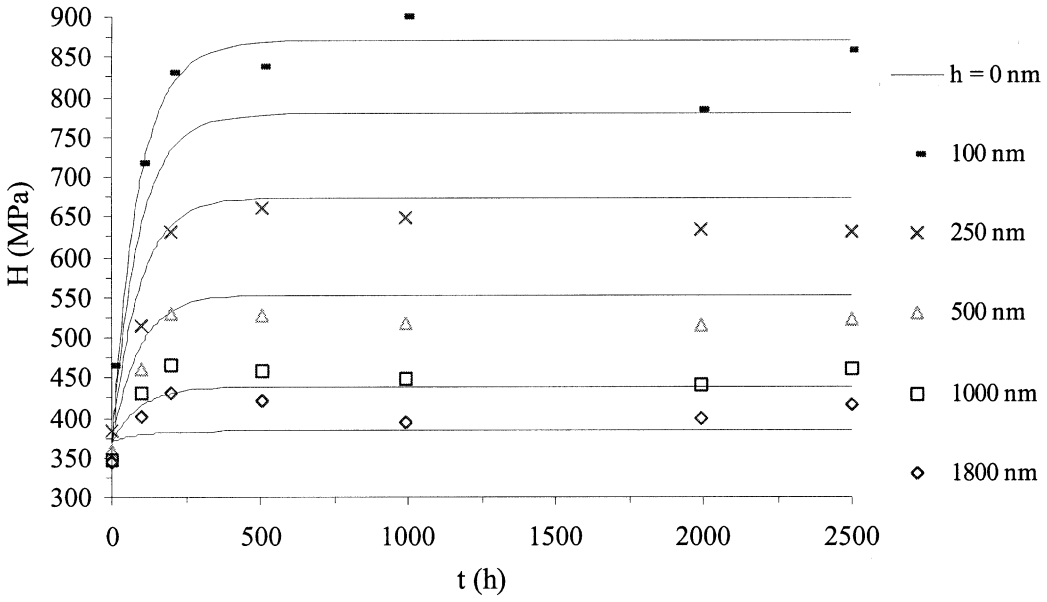

Fig. 16. H versus the irradiation time (different indentation depths)—System II (-, x, Δ, □, ◇: experimental points; curves: model).

$$E_r=\left[\frac{1-\upsilon_f^2}{E_f}\left(1-\exp-\alpha\frac{f_{t_E}}{h}\right)+\frac{1-\upsilon_s^2}{E_s}\exp-\alpha\frac{f_{t_E}}{h}+\frac{1-\upsilon_i^2}{E_i}\right]^{-1} \quad (3)$$

E_f, E_s, E_i: Young's modulus of the film, the substrate and the indenter, respectively,
ν_f, ν_s, ν_i: Poisson coefficients of the film, the substrate and the indenter, respectively,
f_{t_E}: film thickness calculated from Young's modulus evolution,
h: indentation depth,
α: coefficient depending on the shape of the indenter.

In the present case, the term relative to the indenter can be neglected ($E_i=1145$ GPa, $\nu_i=0.07$), which leads to the following equation:

$$E_r=\left[\frac{1-\upsilon_f^2}{E_f}\left(1-\exp-\alpha\frac{f_{t_E}}{h}\right)+\frac{1-\upsilon_s^2}{E_s}\exp-\alpha\frac{f_{t_E}}{h}\right]^{-1} \quad (4)$$

The geometric coefficient α is punch-geometry and indentation-depth dependent. Given that in this study the used indenter was a Berkovich-type indenter (three-sided pyramid), and according to King's analyses [16] for a pyramidal punch, α can be described as:

$$\alpha=1.12\beta^{0.42} \text{ with } \beta=\frac{\sqrt{A}}{f_{t_E}}=\frac{4.95h}{f_{t_E}} \quad (5)$$

Combining Eqs. (4) and (5):

$$\frac{1}{E_r}=\frac{1-\upsilon_f^2}{E_f}+\left(\frac{1-\upsilon_s^2}{E_s}-\frac{1-\upsilon_f^2}{E_f}\right)\exp-2.19\left(\frac{f_{t_E}}{h}\right)^{0.58} \quad (6)$$

When $h\to 0$, the film properties are reached: $E_r=\frac{E_f}{1-\upsilon_f^2}$

When $h\to\infty$, the substrate properties are reached: $E_r=\frac{E_s}{1-\upsilon_s^2}$

With such a theoretical structural model, i.e. a hard film on a softer substrate, the experimental curves $E_r=f(h)$ can be adjusted using Eq. (6). The standard data $\nu_s=\nu_f=0.3$ were chosen to be the Poisson coefficient of the substrate and the film, respectively. Young's modulus for both of the non-oxidised matrixes were:

System I: $E_{S\ I}=5.1\pm0.05$ GPa (DGEBA-MTHPA).
System II: $E_{S\ II}=4.6\pm0.1$ GPa (DGEBA-IPDA).

In that case, E_f and f_{t_E} are the two unknowns of Eq. (6). However, according to the dispersion, the E_f data are quite close to those measured at 50 nm. The calculated values for the unknowns E_f and f_{tE}, are given in Tables 2 and 3. Two examples of adjusted curves are given in Figs. 17 and 18 for systems I and II, respectively. Table 2 shows that E_f increases with the irradiation time t until saturation, as previously observed in Figs. 9 and 15. On the other hand, the f_{t_E} value is relatively constant for each system:

System I: $f_{t_E}=50$ nm.
System II: $f_{t_E}=100$ nm.

In this study, E_f corresponds to the calculated value of Young's modulus at the sample's surface, i.e. when $h\to 0$. If we write $E(t, h)$, the Young's modulus for t and h fixed, then, the modulus of the film E_f is given by $E(t, 0)$ and the substrate E_S by $E(0, \infty)$.

Table 2
Calculated values of E_f and f_{t_E} for the DGEBA-MTHPA matrix

System I ($E_{S\ I} = 5.1$ GPa)

t (h)	0	25	48	75	96	213	246	309	412	530
E_f (GPa)	7.0	8.0	8.8	9.2	9.0	10.4	10.2	10.6	10.4	10.4
f_{t_E} (nm)	50	35	50	50	50	50	50	50	50	50

Table 3
Calculated values of E_f and f_{t_E} for the DGEBA-IPDA matrix

System II ($E_{S\ II} = 4.6$ GPa)

t (h)	0	100	200	506	994	1993	2500
E_f (GPa)	6.5	9.2	11.7	12	12	12	12
f_{t_E} (nm)	5	90	110	100	100	100	100

Figs. 9 (system I) and 15 (system II) show that the evolution of $E(t, 0)$ versus t, follows a typical law:

$$E(t,0) = E(0,0) + (E(\infty,0) - E(0,0))[1 - \exp - \beta_E t] \quad (7)$$

with

$\beta_E = 1.3\ 10^{-2}\ h^{-1}$, $E(0, 0) = 7.0$ GPa and $E(\infty, 0) = 10.4$ GPa (system I).
$\beta_E = 1.1\ 10^{-2}\ h^{-1}$, $E(0, 0) = 4.6$ GPa and $E(\infty, 0) = 12$ GPa (system II).

According to Eq. (6), the evolution versus the indentation depth h of Young's modulus to the limits $E(0, h)$ and $E(\infty, h)$ can be written for $t = 0$ and $t = \infty$ as:

$$E(0,h) = \left[\frac{1}{E(0,0)} + \left(\frac{1}{E(0,\infty)} - \frac{1}{E(0,0)}\right)\exp - \alpha\left(\frac{f_{t_E}}{h}\right)^{0.58}\right]^{-1}$$
$$E(\infty,h) = \left[\frac{1}{E(\infty,0)} + \left(\frac{1}{E(\infty,\infty)} - \frac{1}{E(\infty,0)}\right)\exp - \alpha\left(\frac{f_{t_E}}{h}\right)^{0.58}\right]^{-1} \quad (8)$$

with $f_{t_E} = 50$ nm, $\alpha = 2.19$ and $E(0, 0) = E(\infty, \infty) = 5.1$ GPa.

Combining Eqs. (7) and (8), the expression for Young's modulus versus t and h can be extracted:

$$E(t,h) = E(0,h) + (E(\infty,h) - E(0,h)) \times [1 - \exp - \beta_E t] \quad (9)$$

with $E(0, h)$ and $E(\infty, h)$ given by relations (8).

Therefore, it is possible to plot the kinetics of Young's modulus evolution for each indentation depth studied (Fig. 9—system I). The calculated points are in good agreement with the measurements. However, Fig. 9 reveals that Young's modulus of the non-irradiated sample changes with the indentation depth. In fact, it is possible that a post-ageing occurred at the surface samples after the photo-ageing inside the cell. Thus, the origin of the photo-ageing time has been displaced.

According to the same argument, the post-ageing for system II (unpolished samples) is lower. Indeed, the modulus value of the non-oxidised samples is not very dependent on the indentation depth (Fig. 15). Note that the value $f_{t_E} = 5$ nm for system II (Table 2) confirms this tendency.

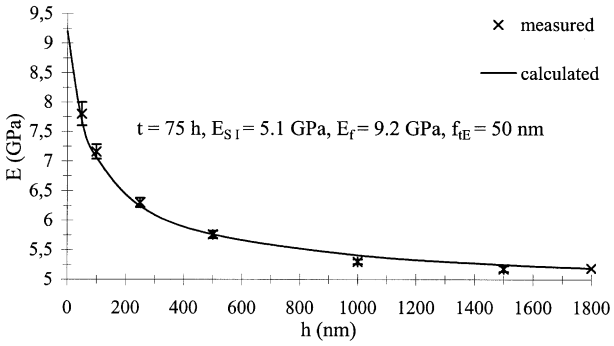

Fig. 17. Example of adjusted curve fort $t = 75$ h of irradiation (System I).

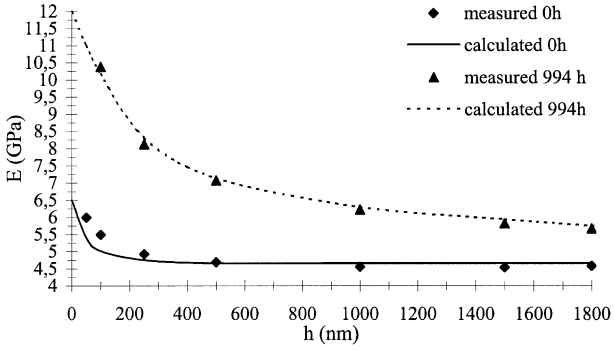

Fig. 18. Example of adjusted curves fort $t = 0$ and 994 h of irradiation (System II).

5.2. *Hardness* H

According to the same protocol described above, we tried to fit the hardness evolution versus the indentation depth by a simple analytical function. In Nano-Indentation, when the substrate is softer than the film, the relation between H and h can be described by the equation [1]:

$$H = H_S + (H_f - H_S)\exp - \gamma h \quad (10)$$

with $\gamma = \frac{H_f}{H_S}\frac{\sigma_S}{\sigma_f}\sqrt{\frac{E_S}{E_f}}\frac{1}{f_{t_H}}$

Table 4
Calculated values of H_f and γ for system I

System I: DGEBA-MTHPA: $H_{s\,I} = 370$ MPa									
t (h)	0	25	48	75	96	213	246	309	530
H_f (MPa)	480	500	560	540	510	520	560	560	540
γ (nm^{-1})	$3.5\ 10^{-3}$	$3.5\ 10^{-3}$	$3/3.5\ 10^{-3}$	$3/3.5\ 10^{-3}$	$3.5\ 10^{-3}$	$3.5\ 10^{-3}$	$3/3.5\ 10^{-3}$	$3.5\ 10^{-3}$	$3.5\ 10^{-3}$

Table 5
Calculated values of H_f and γ for system II

System II: DGEBA-IPDA: $H_{s\,II} = 370$ MPa							
t (h)	0	100	200	506	994	1993	2500
H_f (MPa)	460	650	850	870	860	830	850
γ (nm^{-1})	$4\ 10^{-3}$	$2\ 10^{-3}$	$2\ 10^{-3}$	$2\ 10^{-3}$	$2\ 10^{-3}$	$2\ 10^{-3}$	$2\ 10^{-3}$

H_f, H_s: hardness of the film and the substrate respectively,
σ_f, σ_s: yield strengths,
E_f, E_s: Young's modulus,
f_{t_H}: film thickness calculated from hardness evolution.

An example of the adjusted curves is given in Fig. 19 for system I. The calculated values H_f and γ are given in Tables 4 and 5.

γ Values are of the order of $3\ 10^{-3}$–$3.5\ 10^{-3}$ nm^{-1}, i.e. $1/\gamma = 330$–286 nm for system I. For the system II, $\gamma = 2\ 10^{-3}$ nm^{-1}, i.e. $1/\gamma = 500$ nm. The calculated points are reported in Fig. 20 [$H_f = f(t)$]. In spite of the scatter, H_f increases with the irradiation time t.

According to Eq. (10), f_t is dependent on σ_S/σ_f [Eq. (11)] whose value is unknown.

$$f_{t_H} = \frac{1}{\gamma}\frac{H_f}{H_S}\frac{\sigma_S}{\sigma_f}\sqrt{\frac{E_S}{E_f}} \tag{11}$$

when $\gamma = 3.5\ 10^{-3}$ nm^{-1}, $f_{t_H} = 300\ \frac{\sigma_S}{\sigma_f}$ (system I). When $\gamma = 2\ 10^{-3}$ nm^{-1}, $f_{t_H} = 730\ \frac{\sigma_S}{\sigma_f}$ (system II).

Using the commonly realized hypothesis, $\frac{\sigma_S}{\sigma_f} \sim \frac{H_S}{H_f}$, the two γ values lead to $f_{t_H} = 200$ nm (system I) and $f_{t_H} = 310$ nm (system II).

Using a kinetic law identical to Eq. (7), the hardness evolution with irradiation time t, can be expressed by the relation:

$$H(t,0) = H(0,0) + (H(\infty,0) - H(0,0)) \times [1 - \exp - \beta_H t] \tag{12}$$

Thus, according to Eq. (10), the hardness evolution with the indentation depth for $t = 0$ and $t = \infty$ can be written as:

$$H(0,h) = H(0,0) + [H(0,\infty) - H(0,0)]\exp - \gamma h$$
and
$$H(\infty,h) = H(\infty,0) + [H(\infty,\infty) - H(\infty,0)]\exp - \gamma h \tag{13}$$

Combining Eqs. (12) and (13), the expression of the hardness versus t and h can be extracted:

$$H(t,h) = H(0,0) + (H(\infty,0) - H(0,0)) \times [1 - \exp - \beta_H t] \tag{14}$$

The calculated curves for both analyzed systems are reported in Figs. 10 (system I) and 16 (system II).

To summarize this quantitative analysis, the calculated parameters for both systems are reported in Tables 6 and 7. It shows that for both systems, the β values are about identical. It confirms the similar behaviour of the two epoxy matrixes under photo-oxidative conditions, i.e. a very fast increase in E and H during

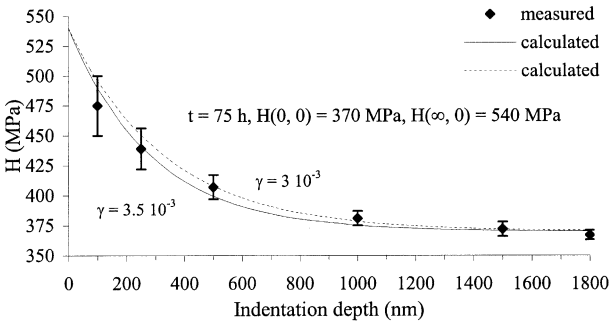

Fig. 19. Example of an adjusted curve for $t = 75$ h (System I).

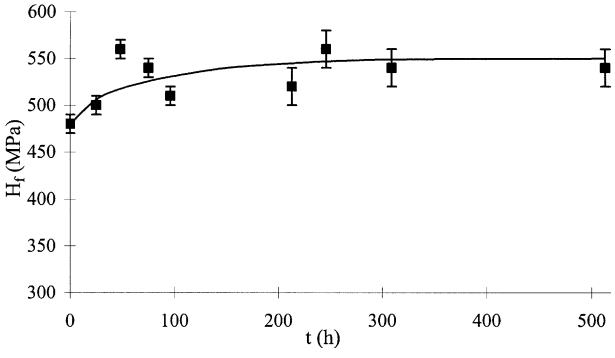

Fig. 20. H_f versus t (System I).

Table 6
Calculated Young's modulus for both epoxy systems

$E(t, h)$						
	$E(0, 0)$ (GPa)	$E(0, \infty) = E(\infty,\infty)$	$E(\infty, 0)$	f_{t_E} (nm)	β_E (h^{-1})	$1/\beta_E$ (h)
System I	7.0	5.1	10.4	50	$1.3\ 10^{-2}$	77
System II	4.6	4.6	12	100	$1.1\ 10^{-2}$	91

Table 7
Calculated hardness for both epoxy systems

$H(t, h)$							
	$H(0, 0)$ (MPa)	$H(0, \infty) = H(\infty, \infty)$	$H(\infty, 0)$	γ (nm^{-1})	$1/\gamma$ (nm)	β_H (h^{-1})	$1/\beta_H$ (h)
System I	480	370	550	$3.5\ 10^{-3}$	280	$1.3\ 10^{-2}$	77
System II	370	370	870	$2.0\ 10^{-3}$	500	$1.1\ 10^{-2}$	91

Table 8
Summary of E and H values

	System I	System II
E_f (GPa)	10.4	12.0
E_S (GPa)	5.1	4.6
H_f (MPa)	550	950
H_S (MPa)	370	370
E_f/E_S	2.0	2.6
H_f/H_S	1.5	2.6

the first 100 h of irradiation and a stabilization once the photo-oxidation layer is established.

Moreover, $f_{t_E}(I)/f_{t_E}$ (II) = 0.5 and $f_{t_H}(I)/f_{t_H}$ (II) = 0.6. These values confirm the previous analyses [4,14], i.e. the ablation coefficient of system I is twice as weak as the one in system II, and the thickness of the photo-oxidation layer is greater for system II than system I.

6. Conclusion

After UV-Visible artificial photo-ageing, the measurements by Nano-Indentation show that the mechanical properties of the analyzed systems (DGEBA-MTHPA and DGEBA-IPDA) changed near the irradiated surface. Indeed, Young's modulus and the hardness of these epoxy matrixes increase similarly with the irradiation time in two separate phases: a very fast increase during the first 100 h and a stabilisation at about 250–300 h. Moreover, this study confirms the presence of a thin photo-oxidation layer (hard film) at the matrix's surface, previously highlighted by physico-chemical analyses [2,12,13]. The minimum and maximum values of E and H are summarized in Table 8.

It was shown that Young's modulus increases with the irradiation time, which is characteristic of the chemical modifications that take place near the matrix's surface. Thus, from a mechanical point of view, the Nano-indentation highlights the photo-chemical degradation effects of these polymeric matrixes.

References

[1] Bhattacharya AK, Nix WD. Int J Solids Struct 1988; 24(12):1287.
[2] Monney L, Bole J, Dubois C, Chambaudet A. Polym Degrad Stab 1999;66:17–22.
[3] Monney L, Dubois C, Chambaudet A. Polym Degrad Stab 1997; 56:357–66.
[4] Guillot L, Monney L, Dubois C, Chambaudet A. Polym Degrad Stab 2001;72:209–15.
[5] Ciba-Geygy Division polymères—Matrix systems. Fiche technique: système de résine époxyde thermodurcissable pour matrice Araldite LY 556. Durcisseur HY 917, Accélérateur DY 070, Avril 1992.
[6] Ciba Specialty Chemicals, Performance Polymers, Structural Composites. Fiche Technique: système matrice pour composites industriels—système époxyde à base d'Araldite LY 556/Durcisseur HY 2962 pour durcissement à chaud, Mars 1998.
[7] J. Floquet. Documentation Original Hanau-Heraeus SA, 1988.
[8] Oliver WC, Pharr GM. J Mater Res 1992;7(6):1564.
[9] Poilane C, Delobelle P, Bornier L, Mounaix P, Melique X, Lippens D. Mater Sci Eng 1999;A262:101–6.
[10] Mounaix P, Delobelle P, Melique X, Bornier L, Lippens D. Mater Sci Eng 1998;B51:258.
[11] Sergent A, Poilane C, Robert L, Delobelle P. J Phys IV France 1998;8:259.
[12] Monney L, Belali R, Vebrel J, Dubois C, Chambaudet A. Polym Degrad Stab 1998;62:353.
[13] Monney L, Rouge N, Dubois C, Chambaudet A. Polym Degrad Stab 1998;62:367.
[14] Monney L, Dubois C, Chambaudet A. Die Angew Makromol Chem 1999;273:6–11.
[15] Mencil J, Munz D, Quandt E, Weppelmann ER. J Mater Res 1997;12(9):2475.
[16] King RB. Int J Solids Struct 1987;23(12):1657.